Available online at www.sciencedirect.com
ScienceDirect
Geochimica et Cosmochimica Acta 72 (2008) 5781–5798
Geochimica et Cosmochimica Acta
www.elsevier.com/locate/gca

A laser probe $^{40}Ar/^{39}Ar$ and INAA investigation of four Apollo granulitic breccias

Jillian A. Hudgins [a,*], John G. Spray [a], Simon P. Kelley [b], Randy L. Korotev [c], Sarah C. Sherlock [b]

[a] Planetary and Space Science Centre, Department of Geology, University of New Brunswick, 2 Bailey Drive, Fredericton, NB, Canada E3B 5A3
[b] Department of Earth and Environmental Sciences, Centre for Earth, Planetary, Space & Astronomical Research (CEPSAR), The Open University, Milton Keynes MK7 6AA, UK
[c] Department of Earth and Planetary Sciences, Washington University, St. Louis, MO 63130, USA

Received 17 October 2007; accepted in revised form 25 August 2008; available online 21 September 2008

Abstract

Infrared laser probe $^{40}Ar/^{39}Ar$ geochronology, instrumental neutron activation analysis (INAA) and analytical electron microscopy have been performed on four $0.5 \times 1.0 \times 0.3$ cm polished rock tiles of Apollo 16 and 17 granulitic breccias (60035, 77017, 78155, and 79215). Pyroxene thermometry indicates that these samples were re-equilibrated and underwent peak metamorphic sub-solidus recrystallization at 1000–1100 °C, which resulted in homogeneous mineral compositions and granoblastic textures.

$^{40}Ar/^{39}Ar$ data from this study reveal that three samples (60035, 77017, and 78155) have peak metamorphic ages of ~4.1 Ga. Sample 79215 has a peak metamorphic age of 3.9 Ga, which may be related to Serenitatis basin formation. All four samples contain moderately high concentrations of meteoritic siderophiles. Enhanced siderophile contents in three of the samples provide evidence for projectile contamination of their target lithologies occurring prior to peak metamorphism.

Post-peak metamorphism, low-temperature (<300 °C) events caused the partial resetting of argon in the two finer-grained granulites (60035 and 77017). These later events did not alter the mineralogy or texture of the rocks, but caused minor brecciation and the partial release of argon from plagioclase. Interpretation of the low-temperature data indicates partial resetting of the argon systematics to as young as 3.2 Ga for 60035 and 2.3 Ga for 77017. Cosmic ray exposure ages range from 6.4 to ~339 Ma.

Our results increase the amount of high-precision data available for the granulitic breccias and lunar highlands crustal samples. The results demonstrate the survival of pre-Nectarian material on the lunar surface and document the effects of contact metamorphic and impact processes during the pre-Nectarian Epoch, as well as the low-temperature partial resetting of ages by smaller impact events after 3.9 Ga.

The mineralogy and chemical composition of these rocks, as well as exhumation constraints, indicate that the source of heat for metamorphism was within kilometers of the surface via burial beneath impact-melt sheets or hot ejecta blankets.
© 2008 Elsevier Ltd. All rights reserved.

1. INTRODUCTION

Lunar granulitic breccias comprise a suite of metamorphic rocks recovered at most Apollo and Luna landing sites and found within non-mare lunar meteorites (e.g., ALHA 81005, SaU 300, NWA 3163/4481/4483). They typically occur as lithic clasts in breccias, but some monolithic rocks have been sampled (e.g., 78155 and 79215). Those occurring as lithic clasts have been incorporated into polymict impact-melt breccias. Their diagnostic feature is a granoblastic to poikiloblastic matrix texture attributed to heating to ~1000 °C, which resulted in sub-solidus recrystallization.

* Corresponding author.
E-mail address: jillian.hudgins@unb.ca (J.A. Hudgins).

0016-7037/$ - see front matter © 2008 Elsevier Ltd. All rights reserved.
doi:10.1016/j.gca.2008.08.024

There is no evidence of plastic deformation and, in this respect, the rocks can be likened to high-temperature terrestrial hornfelses. The source of heat for metamorphism has been debated. Two scenarios appear feasible: (1) heating of the rock due to burial at depth within the lunar crust (deep origin), and (2) juxtaposition with, or burial beneath, hot impact-melt or fallback breccias (shallow origin). Given estimated lunar thermal gradients at ~4 Ga, a deep origin would require depths of metamorphism of ~100 km (e.g., Elkins-Tanton et al., 2004) and an exhumation mechanism to bring this material to surface without significant re-equilibration (i.e., fast). A contact metamorphic (shallow) origin requires heating of footwall material within a few kilometers of the surface in close proximity to overlying superheated impact-melts or related fallback breccias and ejecta. This "aureole" origin avoids the difficulty of exhuming deep crustal rocks and is generally favoured by the community (e.g., Cushing et al., 1999).

Age data for the granulitic breccias is limited. Those that have been dated range from ~3.8 to ~4.2 Ga (Table 1). Most samples are too fine-grained to permit the mineral separation necessary for Rb–Sr or Sm–Nd internal isochron age determinations (Papike et al., 1998 and references therein). Previous step-heating experiments have revealed two dominant age plateaus: one around 4.2 Ga and the other near 4.0 Ga (Phinney et al., 1975; Cadogan and Turner, 1976; Marvin et al., 1987). For those samples, this reveals the timing of the latest thermal metamorphism and/or exhumation prior to the formation of the larger impact basins, such as Imbrium and Serenitatis (Cohen, 2004). Coupled with a lack of contamination by KREEP-rich materials and a bulk composition indicative of ancient upper crust, the granulitic breccias have the potential to provide insight into the Moon's elusive pre-Nectarian crustal history.

To assess whether granulitic ages reflect the time of impact metamorphism or whether granulite metamorphism causes only incomplete de-gassing of ^{40}Ar, Cohen (2004) modeled experimental results and demonstrated that the high temperatures and moderate cooling rates experienced by the granulitic breccias were sufficient to fully de-gas plagioclase. On this basis, the oldest ages of the granulitic breccias represent the date of the peak metamorphic event and not the age of crystallization of the protolith (Cohen, 2004). However, partial de-gassing can also occur at temperatures below the metamorphic peak, resulting in ages younger than the timing of granulite grade recrystallization. Such events are likely to be related to secondary heating by adjacent impact craters or superposition of hot ejecta layers from more distal craters.

Table 1
Summary of existing age data for granulitic impactites

Sample number	^{40}Ar–^{39}Ar (Ga) step-heating	U–Pb (Ga)	Reference
15418,50	3.89 ± 0.06[a]		[a]Stettler et al. (1973)
67215,8	3.75 ± 0.11[b]		[b]Marvin et al. (1987)
67415	3.96 ± 0.04[b]		[b]Marvin et al. (1987)
76235	3.85 ± 0.1[c]		[c] Cadogan and Turner (1976)
77017	3.98 ± 0.1[d]		[d]Kirsten and Horn (1974)
77017,46	3.82 ± 0.02[e]		[e]Phinney et al. (1975)
78155	4.12 ± 0.04[f]	4.22[g]	[f]Turner and Cadogan (1975)
	4.06 ± 0.04[f]		[g]Nunes et al. (1975)
79215	4.03 ± 0.02[h]		[h]McGee et al. (1978)
	3.91 ± 0.1[i]		[i]Oberli et al. (1979)

Ages measured before 1977 have been corrected to the decay rates of Steiger and Jäger (1977).

Compositionally, the granulitic breccias can be divided into ferroan (plagioclase > pyroxene > olivine) and magnesian (plagioclase > olivine > pyroxene) groups. Both typically comprise >80% plagioclase, hence the use of the term feldspathic granulitic breccias by some researchers (e.g., Warner et al., 1977). They exhibit moderately high siderophile element concentrations indicative of projectile contamination. The Mg/Fe ratios for granulitic breccias are almost dichotomous. Ferroan varieties possess Mg# 50–72 and magnesian granulites have Mg# 73–85 (Table 2) (Lindstrom and Lindstrom, 1986). Scandium contents and Cr/Sc ratios define these two groups even more precisely. Ferroan granulites have approximately twice as much Sc as magnesian granulites. Compositionally, ferroan granulitic breccias are consistent with derivation from ferroan anorthosite (FAN) rocks, but magnesian granulitic breccias are not compositionally consistent with a mixture of any of the known Mg-suite lithologies (Korotev et al., 2003).

Although their bulk compositions resemble the average composition of lunar highlands crust (Korotev et al., 2003), all granulitic breccias are contaminated with meteoritic siderophiles (Table 2). Granulitic breccias have low but variable abundances of incompatible trace elements, distinguishing them from most other Apollo polymict breccias (Lindstrom and Lindstrom, 1986).

In this study, we present the results of a petrological, chemical, and ^{40}Ar/^{39}Ar geochronological study of four Apollo suite granulitic breccias: sample 60035 from Apollo 16, and samples 77017, 78155, and 79215 from Apollo 17, with a focus on the relationship between grain size, age, and siderophile element concentration. The goal is to provide further data on the timing of impact events in the early lunar highlands crust, to constrain the origins of the lunar granulitic breccias, and to explore the timing of their latest episodes of thermal metamorphism.

2. EXPERIMENTAL METHODS

2.1. Sample preparation and microscopy

The four samples (60035, 77017, 78155, and 79215) were selected because they cover the range of fine- to coarse-grained, poikiloblastic to granoblastic, and ferroan to magnesian granulitic breccias. Each of the four samples was prepared as a ~0.3 mm thick, ~0.5 cm × 1 cm polished thick section, which was photographed with a digital camera to provide a map of the distribution of clasts and matrix (Fig. 1a–d). A thin section was made from the adjacent slice of each rock. The four thin sections were examined with a Nikon E400 optical microscope using transmitted and reflected light to determine grain size and texture. Back-scattered electron (BSE) images and

Table 2
Average bulk compositions of the four granulitic breccia samples compared to other crustal lithologies

	60035 GB	77017,2 GB	78115,2 GB	79215,1 GB	60025,45 FAN	72255,c2 N	72275,91 A17K
SiO_2	46.49	44.09	45.57	43.4	45.3	52	48
TiO_2	0.2	0.41	0.27	0.13	0.02	0.3	1.4
Al_2O_3	26	26.59	25.94	28.5	34.2	15.5	13.5
Cr_2O_3	0.11	0.13	0.14	0.07	0.004	0.161	0.46
FeO	4	6.19	5.82	4.3	0.5	7.4	15
MnO	0.05	0.08	0.1	0.04	0.008	0.122	0.156
MgO	8.4	6.06	6.33	6.3	0.21	15.9	10
CaO	14.3	15.43	15.18	15.9	19.8	9.1	10.5
Na_2O	0.38	0.3	0.33	0.04	0.45	0.33	0.29
K_2O	0.07	0.06	0.08	0.09	0.113	0.08	0.25
Type	Magnesian	Ferroan	Ferroan	Magnesian			
Mg#	80	68	68	77	43	81	54
	Ma and Schmitt (1982)	LSPET (1973)	LSPET (1973)	McGee et al. (1978)	Papike et al. (1998) and references therein	Papike et al. (1998) and references therein	Papike et al. (1998) and references therein
	GB, granulitic breccia	FAN, ferroan anorthosite	N, norite	A17K, Apollo 17 KREEP			

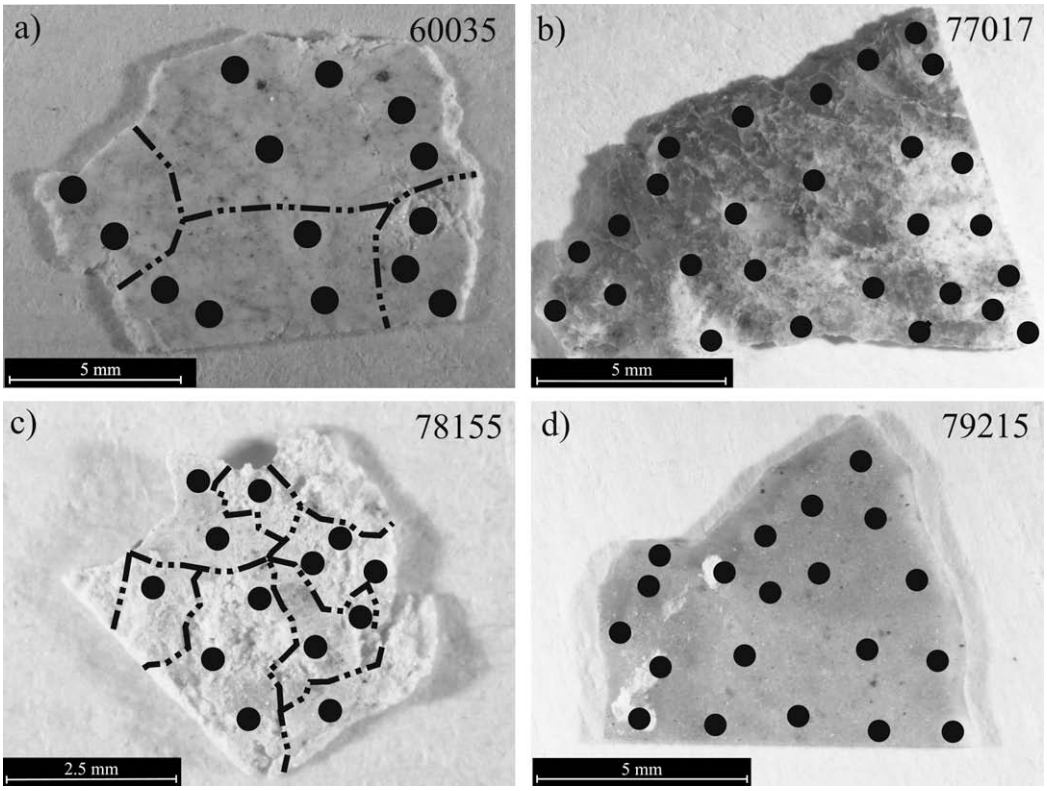

Fig. 1. Photographs of the tiles in reflected light (a) 60035, (b) 77017, (c) 78155, and (d) 79215. Dashed lines represent where the samples broke, circles represent the positions of IR laser spots.

quantitative analysis of the matrix and mineral and lithic clasts were obtained using a JEOL 6400 digital analytical scanning electron microscope (ASEM) equipped with an EDAX Phoenix X-ray microanalysis system, Sapphire Si (Li) detector, and Genesis microanalysis software. Operating conditions were 15 kV accelerating voltage, 1.5 nA current, and 14 mm working distance. ZAF corrections were applied to all analyses, which were calibrated using a multi-element standard block (Type 202–52). Counting times were 50 s. Pyroxene compositions were analyzed for thermometry calculations using a JEOL JXA-733 electron microprobe (EMP) equipped with four wavelength

dispersive spectrometers (WDS) at an accelerating voltage of 15 kV and a beam current of 15 nA. Minerals were analyzed using a 1 μm spot size.

The samples were then cleaned in methanol and de-ionized water prior to being packaged in aluminum foil and irradiated at the McMaster University Research Reactor (Canada) for 100 h. The fast neutron flux (5×10^{18} n/cm^2) was monitored using biotite standard GA1550 and amphibole standard Hb3Gr, with an age of 1072 Ma (Turner, 1970) and a calculated J value of 0.03475 ± 0.00002.

2.2. IR laser microprobe $^{40}Ar/^{39}Ar$ analysis

In situ laser microprobe $^{40}Ar/^{39}Ar$ spot analysis was performed at The Open University, Milton Keynes (UK), using a CW 1090 nm fiber laser focused through a Leica petrological microscope with a computer-controlled shutter. Each analysis was made using infrared laser pulses of 50 or 75 ms duration at a laser power of 0.4 W. Resulting laser pits were between 50 and 100 μm in diameter. Pit depths are approximately half of the pit diameter (i.e., 25–50 μm). Active gases were removed by two SAES AP 10 getters, one operating at 400 °C and one at room temperature (residence time in getters was 5 min). The remaining noble gases were then admitted into an MAP 215–50 noble gas mass spectrometer and analyzed isotopically. Blanks were analyzed after every two analyses. Blanks were determined using the same extraction process but without firing the laser. The relative abundances of ^{40}Ar, ^{39}Ar, ^{38}Ar, ^{37}Ar, and ^{36}Ar were measured by the mass spectrometer ten times in sequence over a period of ~15 min. Peak intensities were extrapolated back to inlet time and corrected for blanks, mass spectrometer discrimination, and reactor-induced interferences. The correction factors used were $(^{39}Ar/^{37}Ar)_{Ca} = 0.00065$, $(^{36}Ar/^{37}Ar)_{Ca} = 0.000264$, and $(^{40}Ar/^{39}Ar)_{K} = 0.0085$ based on analyses of Ca and K salts. Typical blank values are $^{40}Ar = 1 \times 10^{-12}$ cc STP, $^{39}Ar = 0.006 \times 10^{-12}$ cc STP, $^{38}Ar = 0.01 \times 10^{-12}$ cc STP, $^{37}Ar = 0.48 \times 10^{-12}$ cc STP, and $^{36}Ar = 0.035 \times 10^{-12}$ cc STP.

A total of 76 $^{40}Ar/^{39}Ar$ spot analyses were obtained from the four samples (Appendix A). In each case the laser probe was positioned within mineral grains; no melt veins were analyzed (present in samples 60035 and 77017 only). Two of the samples had broken into two or more pieces during transport and irradiation, but this did not affect their analysis.

Laser step-heating experiments were also performed on all four samples using the same laser but incorporating a beam splitter to reduce the laser power by 95% (Appendix A). Heating steps were achieved by increasing the laser power from 0.05 to 1 W and rastering the beam over the surface for ~30 s at each step. Fusion and total de-gassing was achieved at ~2000 °C. Blanks were measured after every two steps and a mean of all the blanks was used to calculate the background levels of gases.

2.3. Instrumental neutron activation analysis

For INAA (instrumental neutron activation analysis) we were allocated (via JSC) two splits each of samples 60035, 77017, 78155, and 79215. We prepared two sub-splits of each split (A and B, Table 4) for a total of four subsamples of each sample. Analyzed subsample masses were 100–150 mg each. Samples were encapsulated in high-purity silica tubing and irradiated for 24 h in a thermal neutron flux of 5×10^{13} cm^{-2} s^{-1} in the University of Missouri Research Reactor. Each sample was then radio-assayed by gamma-ray spectrometry four times at Washington University, Missouri: at 6 days, 7–8, 9–11, and 24–28 days following irradiation. Further details of the INAA method are described in Korotev (1991).

3. PETROGRAPHY AND MINERALOGY

The four granulitic breccias exhibit considerable textural and chemical variation (Fig. 1). All are composed of anorthitic plagioclase, low-Ca clinopyroxene, high-Ca clinopyroxene, and olivine with minor (<1%) amounts of Fe-rich metal, ilmenite, Cr-spinel, phosphates, and trace amounts of other accessory minerals. Mineral chemistry is homogeneous on a millimeter scale and there is a characteristic lack of zoning in both clasts and matrix minerals. Lithic clasts are almost entirely feldspathic, although both FAN and magnesian feldspathic rocks are present (Fig. 2). The parental polymict impact breccias probably contained clasts from both suites and were formed as a result of mixing by impact (James, 1980). However, the granulitic breccias are not easily explained as mixtures of known igneous or plutonic rocks on the basis of composition (see discussion of trace elements). Korotev et al. (2003) suggest that their precursors might have contained mixtures of igneous rock types that have not yet been recognized within the Apollo sample suite.

The granulitic breccias studied here range from fine- to coarse-grained and exhibit poikiloblastic to granoblastic textures, as described for other granulitic breccias (e.g., James and Hammarstrom, 1977; Bickel and Warner, 1978). Most samples consist of a mosaic of grains whose boundaries meet at 120° triple junctions, a texture that is produced via sub-solidus recrystallization and grain coarsening (Papike et al., 1998 and references therein; Cushing et al., 1999). The present suite is composed of two distinct textural varieties: coarser poikiloblastic types and finer-grained granoblastic types. Poikiloblastic breccias comprise subhedral to euhedral plagioclase crystals with smooth boundaries, which enclose olivine blebs, and are themselves enclosed in pyroxene oikocrysts (Fig. 3a and b). Granoblastic granulites are dominated by polygonal to rounded, equant grains of annealed anorthite (70–80 vol %) that meet at triple junctions (Fig. 3c and d) (Bickel and Warner, 1978; Cushing et al., 1999).

3.1. Sample 60035

Sample 60035 is a fine-grained, polymict, clast-rich granulitic breccia (Fig. 3a) (Ma and Schmitt, 1982). Its matrix ranges from annealed cataclastic to poikiloblastic textures and its grain size is variable (30–100 μm). It is dominated by mineral clasts (up to 200 μm) of anorthite, olivine, high-Ca clinopyroxene, and orthopyroxene. Accessory

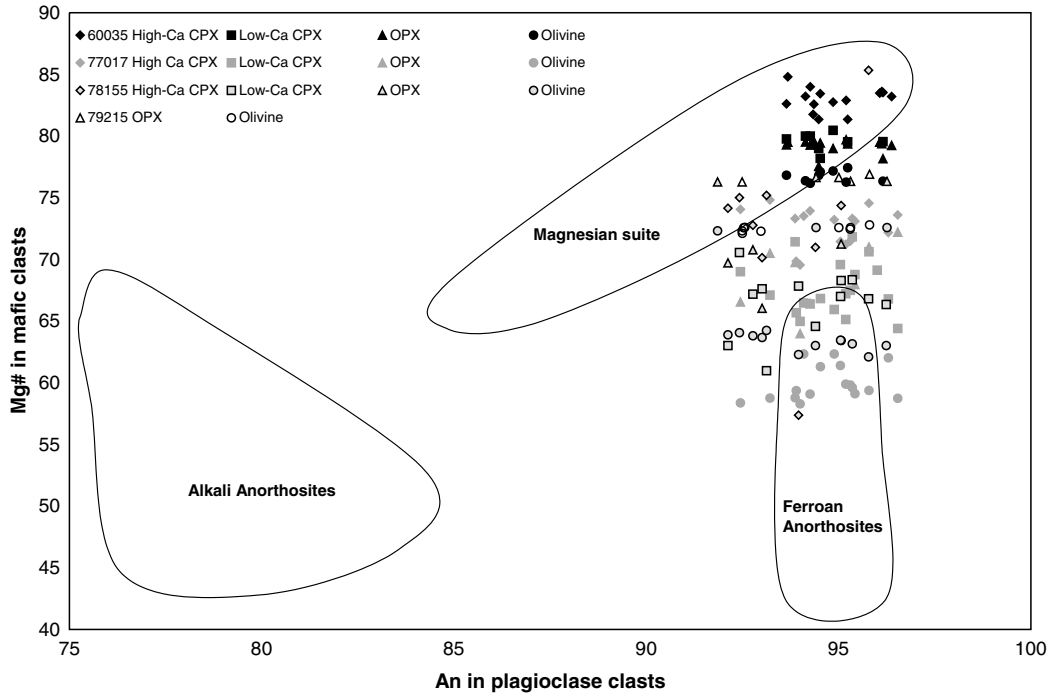

Fig. 2. Mg# (molar Mg/(Mg + Fe) × 100) in mafic minerals (olivine and pyroxene) versus An (molar Ca/(Ca + Na + K) × 100) in feldspar for minerals present in the lithic clasts observed in the four studied granulitic breccias. Fields are for the pristine rock suites (Warren et al., 1983).

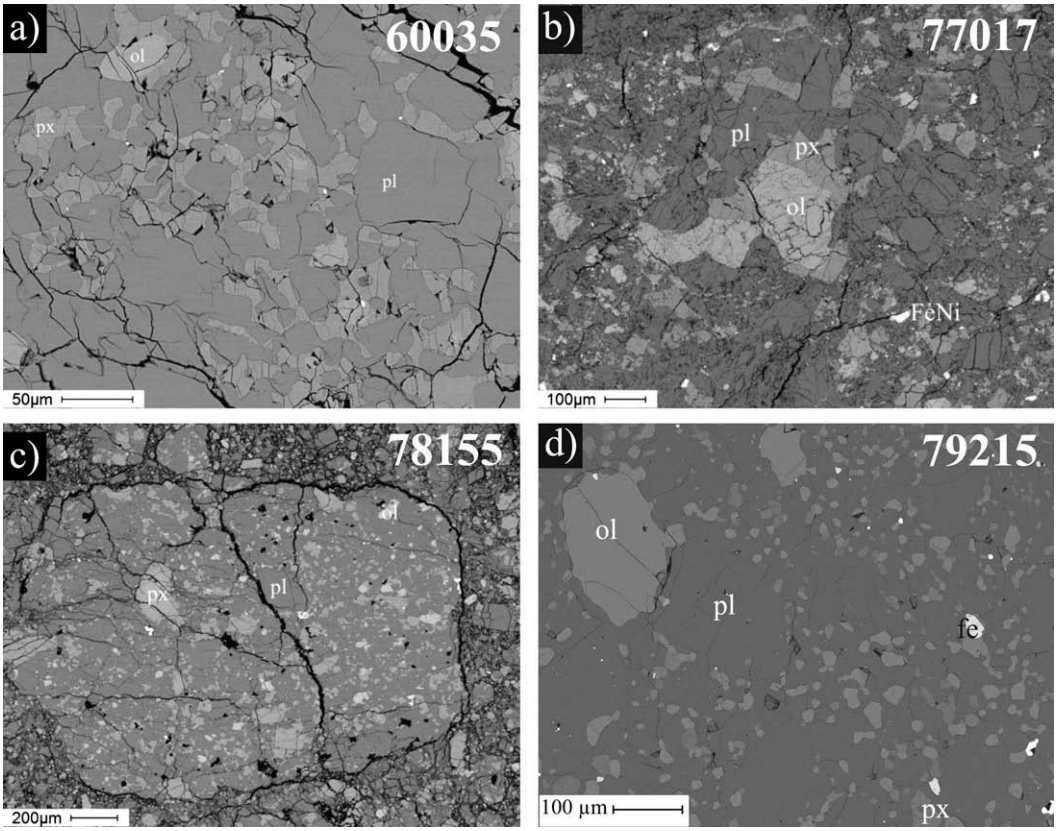

Fig. 3. Backscattered electron images of the four granulitic breccias (a) 60035, (b) 77017, (c) 78155, and (d) 79215. Abbreviations are as follows: pl, plagioclase; ol, olivine; fe, Fe-rich metal; px, pyroxene; and FeNi, FeNi metal.

matrix minerals include low-Ca clinopyroxene, ilmenite, chromite, apatite, zirconalite, and Fe-rich metal. 60035 contains coarser-grained lithic clasts of granoblastic anorthositic troctolite and poikiloblastic anorthositic norite, which grade into the matrix of the rock. A few thin (<10 μm) shock veins are observed (Ma and Schmitt, 1982). These veins were generated after the sample was thermally metamorphosed as they cut through the annealed grains.

Plagioclase mineral fragments enclose chains of rounded mafic minerals along their boundaries, which may indicate the location of their pre-metamorphic grain boundaries (cf., Papike et al., 1998 and references therein). Plagioclase compositions are homogenous ($An_{92–97}$) and no zoning is observed. High-Ca clinopyroxene exhibits a limited range in composition ($Wo_{35–44}En_{47–54}Fs_{9–12}$); low-Ca clinopyroxene has a compositional range of $Wo_{6–13}En_{70–75}Fs_{17–19}$, and orthopyroxene has a restricted compositional range of $Wo_{2–5}En_{75–77}Fs_{19–21}$. Olivines have homogenous compositions ($Fo_{76–78}$) throughout the sample. Fe-rich metal grains contain 4.4–6.1% Ni and 0.9–1.4% Co. The potassium-bearing phase in this sample is plagioclase with an average of 0.13 wt% K_2O.

3.2. Sample 77017

Sample 77017 is a poikiloblastic granulitic breccia with a fine-grained matrix (Meyer, 1994) that has been subsequently disrupted by cataclasis (Fig. 3b), indicating that the rock underwent cold brecciation without plastic shear after it was heated. The sample contains abundant coarse-grained, feldspathic lithic clasts and fractured, subrounded mineral clasts of plagioclase, olivine, spinel, and accessory minerals enclosed in pyroxene oikocrysts up to 1.5 mm wide. Accessory phases include ilmenite, spinel, troilite, and Fe-rich metal. Lithic clasts are mainly relics of anorthosite and noritic anorthosite. This sample displays numerous fracture systems and thin (<10 μm) shock veins are observed (Meyer, 1994). Meyer (1994) concluded that the rock had been strongly shocked and invaded by coarse glass veins. These veins formed after the sample underwent primary thermal metamorphism.

Plagioclase exhibits a restricted compositional range ($An_{92–97}$). Some anorthite fragments contain small (<25 μm) grains of olivine or, rarely, pyroxene. Pyroxene oikocrysts are typically homogeneous. High-Ca clinopyroxene oikocrysts and mineral clasts have compositions of $Wo_{21–42}En_{43–57}Fs_{15–22}$. Low-Ca clinopyroxene oikocrysts exhibit a range of $Wo_{5–17}En_{58–66}Fs_{25–34}$. Orthopyroxene yields restricted compositions of $Wo_{3–5}En_{61-71}Fs_{26–35}$. Olivine mineral fragments range in composition from Fo_{58} to Fo_{62}. No major element zoning was observed in any mineral phase. Ilmenite is the most common oxide phase and is enriched in MgO (3.1–4.9 wt%). Both Cr- and Ti-rich spinels are observed. Fe-rich metal is most commonly intergrown with troilite, but is also observed as independent grains and intergrown with spinel, ilmenite, or olivine. Metal compositions are heterogeneous with 6.3–23.7% Ni and 1.4–2.1% Co. The potassium-bearing phase in 77017 is plagioclase with an average of 0.10 wt% K_2O.

3.3. Sample 78155

Sample 78155 is a holocrystalline, polymict, granoblastic granulitic breccia of anorthositic norite bulk composition (Bickel, 1977). Most of the rock (~65%) has a granoblastic matrix consisting of anorthite, low-Ca and high-Ca clinopyroxene, olivine, and accessory minerals (Fig. 3c). Accessory matrix phases include ilmenite, troilite, a variety of spinels, and Fe-rich metal. The matrix occurs in subangular to subrounded fragments, up to a few millimeters across, separated by curved fractures and regions of crushed material (Bickel, 1977). One of these large fragments was analyzed with the IR laser probe (discussed later). The matrix grain size of the fragments is <150 μm. The rock contains a substantial amount of crushed material (1–100 μm), which comprises up to 20% of the section, in veins or irregularly shaped regions. The late brecciated material has the same composition as the material it was generated from; therefore, this material was formed by late post-metamorphic brecciation, possibly during the event responsible for the exhumation of the sample. This late brecciated material was not part of the thick section, only unbrecciated fragments were analyzed with the laser probe.

The potassium-bearing mineral is plagioclase (average 0.18 wt% K_2O). Plagioclase matrix grains have a compositional range of $An_{89–97}$, a much wider range than is observed in the other granulitic breccias studied here. Compositions of plagioclase mineral clasts range from $An_{92–94}$. Plagioclase grains commonly contain chains of mafic minerals. High-Ca and low-Ca clinopyroxene matrix grains have compositions of $Wo_{16–40}En_{45–53}Fs_{15–30}$ and $Wo_{7–13}En_{59–64}Fs_{27–31}$, respectively. Mafic silicates are located primarily along plagioclase grain boundaries and at triple junctions. The most abundant mafic mineral clast is low-Ca clinopyroxene ($Wo_{6–14}En_{53–63}Fs_{27–34}$). High-Ca clinopyroxene clasts ($Wo_{16–39}En_{45–51}Fs_{16–35}$) are numerous, but orthopyroxene ($Wo_4En_{63–67}Fs_{29–32}$) is rare. Olivine matrix grains exhibit a compositional range of $Fo_{61–66}$. Olivine mineral fragments have compositions between $Fo_{62–66}$. Four compositional groups of spinel were observed; all lie within the chromite–ulvöspinel–hercynite field. Ti-rich chromite is the most abundant type, but Ti–Fe–Al-rich, Fe–Ti–Cr-rich, and Fe–Al–Cr-rich spinels are also present. Ilmenite grains are common and have high MgO contents (2.8–7.1 wt%). Rare grains of apatite and REE-merrillite are present (<15 μm). Merrillite grains are enriched in Ce_2O_3 (1.44 wt%) and Nd_2O_3 (0.7 wt%), while apatite grains contain an average of 1.1 wt% F and 3.8 wt% Cl. The compositions of Fe-rich metal grains range from 3.8% to 9.1% Ni and 1.0% to 2.5% Co. Two large (50 μm) metal grains contain 28% Ni and 2.5% Co.

3.4. Sample 79215

79215 is a holocrystalline, polymict granulitic breccia with a granoblastic matrix comprising anorthite, pyroxene, olivine, and minor apatite, ilmenite, spinel, troilite, zircon, and Fe-rich metal (Fig. 3d) (Bickel et al., 1976). Mineral fragments include mono- and polycrystalline grains of

anorthite and minor olivine, clinopyroxene, and orthopyroxene. Compositional zoning was not detected in any of the major phases. Lithic clasts are mostly anorthositic (Bickel et al., 1976). They comprise fine-grained, polygonal plagioclase. We also observed gabbroic clasts that were not easily distinguishable from the matrix. The main potassium-bearing mineral is plagioclase with an average of 0.11 wt% K_2O.

Anorthite is the most abundant fragment and displays the greatest range in size. We observed no compositional differences between plagioclase in the mineral fragments and the matrix; both have compositional ranges of $An_{92–96}$. Small (<10 μm), round olivine and pyroxene grains are, in places, observed along the rims of anorthite grains, forming irregular chains. Olivine mineral fragments and matrix grains exhibit extremely restricted compositions from $Fo_{72.1}$ to $Fo_{72.8}$. Pyroxene fragments are less common. High-Ca clinopyroxene ($Wo_{41–44}En_{46–49}Fs_{10–11}$) is rare. Orthopyroxene compositions fall within a restricted range ($Wo_{3–4}En_{73–75}Fs_{22–23}$). The compositions of pyroxene fragments and matrix grains are identical. Spinel grains are rich in Cr_2O_3 (37–47 wt%) and contain up to 19 wt% TiO_2. Fe-rich metal compositions are heterogeneous throughout the rock, exhibiting ranges in Co (1.1–1.9%) and Ni (8.6–16.6%) contents.

4. ANALYTICAL RESULTS

4.1. IR laser spot analysis

The four samples are distinct in terms of $^{40}Ar/^{39}Ar$ IR laser spot results. Sample 60035 has an age range of 3638 ± 38 to 3783 ± 36 Ma from 14 individual spots, with ages approximately equally spread over the entire range (Fig. 4a). Sample 77017 is the youngest sample. Its 27 individual spot ages show a much greater span from 3072 ± 18 to 3532 ± 28 Ma (Fig. 4b), with ages equally distributed within that range. Sample 78155 yields the oldest ages and the smallest age variation, from 4080 ± 17 to 4201 ± 26 Ma (Fig. 4c). Sample 79215 yields ages within the range of 3813 ± 20 to 4020 ± 50 Ma from 20 individual spots (Fig. 4d).

4.2. IR laser step-heating analysis

Small pieces (several mm^2) of each of the four tiles were also subjected to IR laser probe step-heating. Release spectra are shown in Figs. 5 and 6.

The release spectrum for sample 60035 yields variable ages, from 3237 ± 201 to 4076 ± 105 Ma. These ages result in a rising staircase of ^{39}Ar fractions, from the youngest age

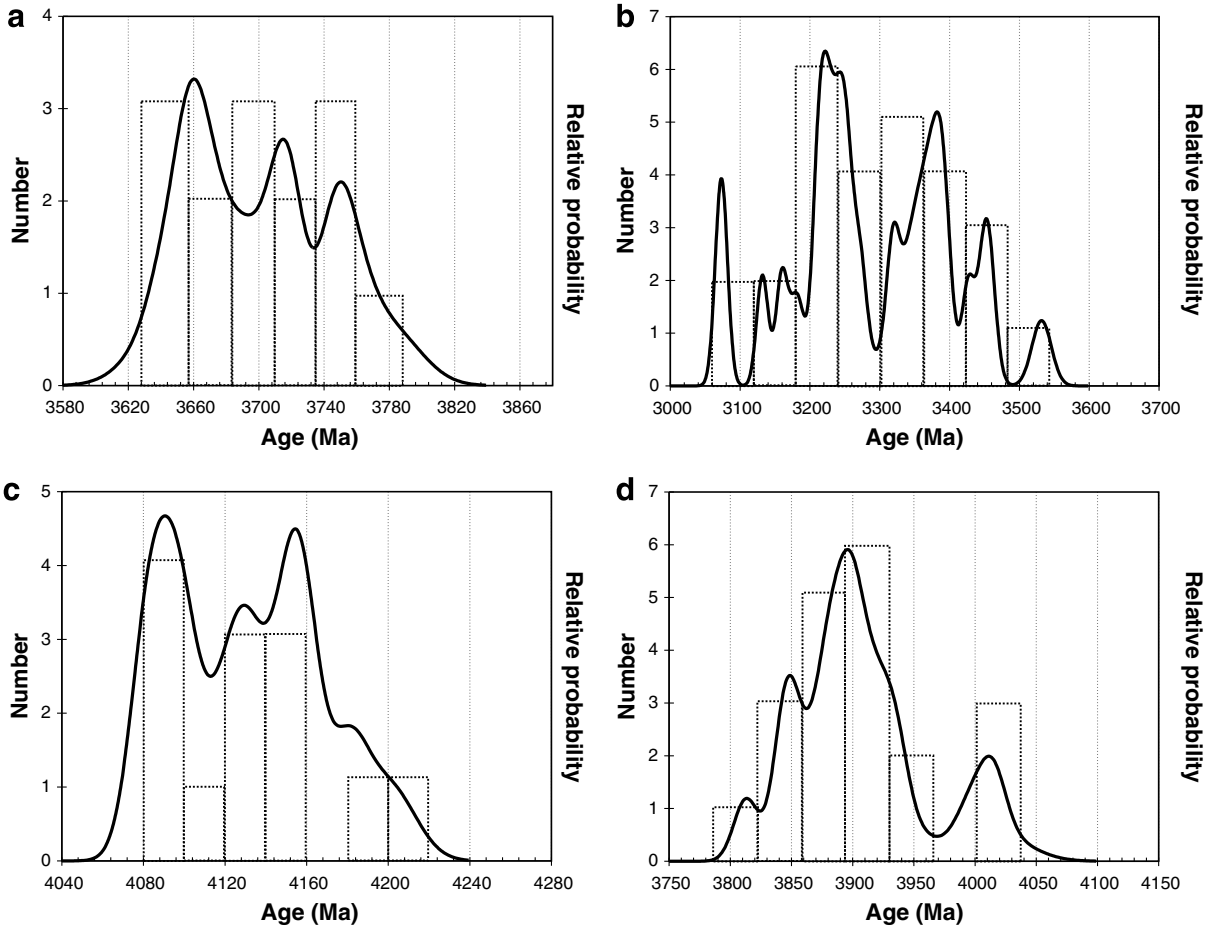

Fig. 4. Relative probability plots based on $^{40}Ar/^{39}Ar$ laser spot ages. (a) 60035, (b) 77017, (c) 78155, and (d) 79215.

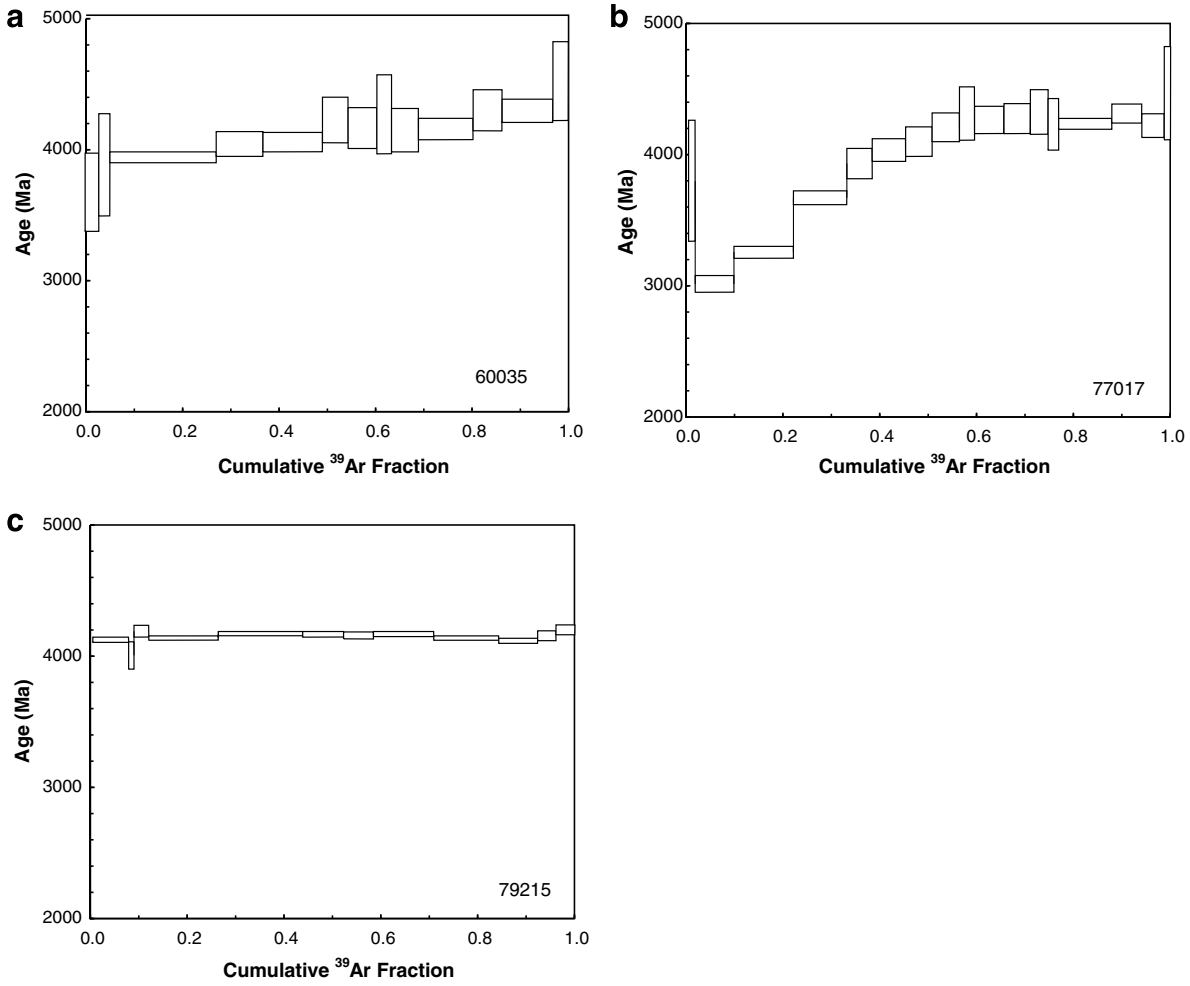

Fig. 5. Step-heating release spectra for samples (a) 60035, (b) 77017, and (c) 79215. Box heights are 2σ.

to a sub-plateau in the final three steps with a mean age of 4088 ± 100 Ma (Fig. 5a). We will return to the shape of the release pattern, which appears to indicate partial loss of a significant proportion of the radiogenic argon at around 3200 Ma.

The release spectrum for sample 77017 yields individual release step ages ranging from 2341 ± 43 to 4108 ± 116 Ma. The release pattern displays a upwardly convex curved pattern characteristic of minor radiogenic argon loss. This pattern indicates that the rock first cooled around 4016 ± 39 Ma (mean of the final ten steps) and was later partially reset at ~2300 Ma (Fig. 5b). Our age of 4016 ± 39 Ma is older than the ages obtained by Kirsten and Horn (1974) (3980 Ma) and by Phinney et al. (1975) (3820 ± 20 Ma), but given the argon loss, the values are not significantly discrepant. Ages measured before 1977 have been corrected to the decay rates of Steiger and Jäger (1977).

The release spectrum of sample 79215 does not indicate a trend toward higher ages with increasing release, but the data are more scattered than demanded by the standard criteria for a plateau (concordant ages from more than 50% of the ^{39}Ar release and more than three temperature steps). The release pattern does not indicate significant argon loss, and yields a total gas age of 3874 ± 16 Ma and a mean age of 3871 ± 40 Ma (Fig. 5c). Individual release steps range from 3676 ± 72 to 3940 ± 24 Ma. The lowest temperature release steps correspond to the first 10% of the spectrum. A similar disturbance appears in the final 10% of the spectrum, yielding older ages. Our age data for sample 79215 compare well with those of Oberli et al. (1979), who obtained an ^{40}Ar/^{39}Ar age of 3910 Ma for this sample. However, our age is slightly younger than that obtained by McGee et al. (1978) who obtained an age of 4030 ± 20 Ma. Although this sample did not yield data sufficiently precise to define a plateau, we will later present evidence for a robust age and errors of 3900 ± 100 Ma.

Sample 78155 yielded little age variation and the data conform to the criteria for a ^{40}Ar/^{39}Ar age plateau. The individual release steps range in age from 4007 ± 32 to 4287 ± 43 Ma (Fig. 6a). Like 79215, this sample exhibits lower temperature release ages in the first 10% of the spectrum. A similar disturbance appears in the final 10% of the spectrum, which yields slightly older ages. The middle portion of the spectrum, corresponding to ~800–1000 °C, yields a plateau age of 4106 ± 43 Ma, comprising 83.8% of the ^{39}Ar released represented by 13 consecutive steps and an MSWD of 0.97 (calculated using Isoplot 3, Ludwig

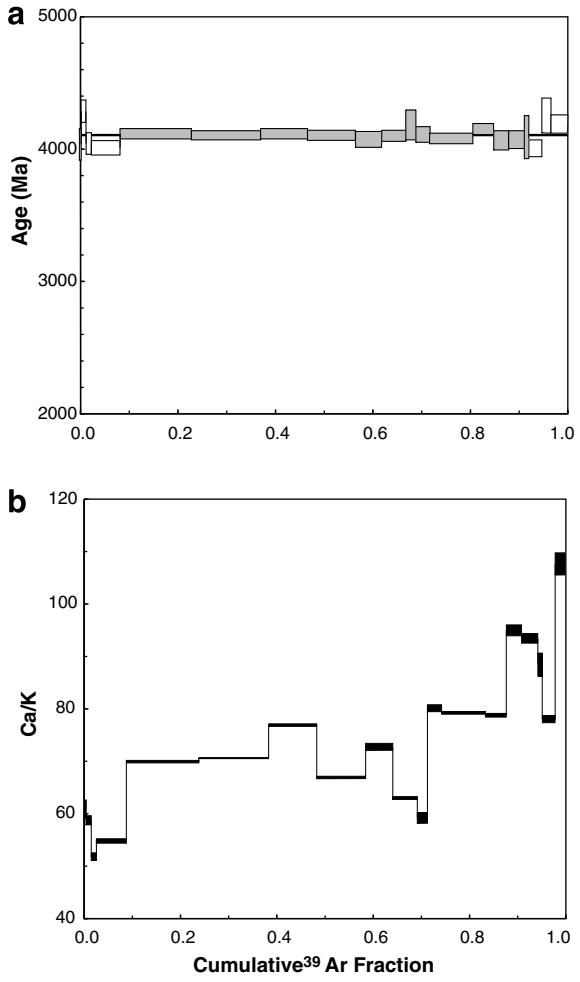

Fig. 6. (a) Step-heating plateau for sample 78155. Plateau age is 4106 ± 43 Ma. Plateau steps are dark grey, rejected steps are light grey. Box heights are 2σ, including J-error of 1%. MSWD = 0.97, probability = 0.47. (b) Ca/K ratios for sample 78155. Box heights are 2σ.

2003). The error on the plateau age is reported at the 2σ level. Comparing this with the Ca/K release spectrum (Fig. 6b), the lowest temperature release steps have the lowest Ca/K ratios (~60) and the highest temperature release steps have the highest Ca/K ratios—as high as 110. Although they fall outside the 2σ errors, our age data for sample 78155 compare well with those of Turner and Cadogan (1975), who obtained an $^{40}Ar/^{39}Ar$ age of 4120 ± 40 Ma and with Nunes et al. (1975) who obtained an U–Pb age of 4.22 Ga for this sample. This indicates that 78155 is internally well-behaved. Ages measured before 1977 have been corrected to the decay rates of Steiger and Jäger (1977).

4.3. Cosmic ray exposure ages

For most lunar rocks, their cosmic ray exposure (CRE) age corresponds to the time at which they were brought to the surface via processing resulting from asteroid impacts rather than tectonic movements (e.g., Eugster, 2003). CRE ages presented here are calculated based on the spallogenic ^{38}Ar content of the sample (Eberhardt et al., 1970). In irradiated samples, ^{38}Ar may also be present as a result of neutron interactions with chlorine. These effects must be considered before any interpretation can be applied to the measured abundances. We have assumed that the samples have had 2π of exposure because they lay on the lunar surface with only their upper surface irradiated by cosmic rays (whereas fully exposed meteoroids have 4π). The CRE ages represent integrated durations of exposure of the rocks close to the surface of the Moon and probably reflect processing during recent impact events. At the near surface samples may exhibit a history including both exposure and burial, in which case the integrated exposure history reflected in the ages is a continuum of such burial and exposure events. In addition, the age assumes that the samples were not affected by shielding by topography. The individual ^{38}Ar production rates were calculated based on the composition of the individual samples using standard production values for Ca, Fe, Ti, and K (Weilerm, 2002 and references therein) and range from 9.46 to 9.85×10^{-9} cm^3 STP/g Ma. CRE ages are given in Table 3.

Table 3
Cosmic ray exposure ages for the four granulitic breccias

Sample number	CRE age (Ma)	±
60035	6.4	0.5
77017	133	9.5
78155	20.7	1.5
79215	339	24.2

4.4. Pyroxene thermometry

Pyroxene thermometry calculations determined from electron microprobe (EMP) analyses of co-existing low- and high-Ca pyroxenes (based on the method of Brey and Köhler (1990)) reveal equilibration temperatures for the four granulitic breccias studied here to be within the range of 990 to 1100 ± 50 °C. There were no notable differences between the calculated equilibration temperatures for poikiloblastic and granoblastic granulitic breccias.

4.5. Geochemistry

For a given sample, concentrations of trace elements and, in particular, siderophile elements (Co, Ni, Ir, and Au) are consistent among subsamples within analytical uncertainty (Table 4). Concentrations of gold are below detection limits for some subsamples. For the Apollo 17 samples, Ir/Au is consistent with the 3/1 ratio typical of ordinary chondrites (Wasson and Kallemeyn, 1988). For the Apollo 16 sample (60035), the ratio is somewhat greater (4–5) and more in the range of CO and CV chondrites, and similar to sample 67475 in this regard (Hertogen et al., 1977). Geochemical constraints on the protoliths to the granulitic breccias are discussed in the next section.

Table 4
Trace element concentrations for the four granulitic impactites determined by INAA

		60035,59 A	60035,59 B	60035,58 A	60035,58 B	77017,186 A	77017,186 B	77017,188 A	77017,188 B	78155,164 A	78155,164 B	78155,166 A	78155, 166 B	79215, 124 A	79215,124 B	79215, 125,A	79215, 125,B	Unc. (2σ, %)
Sc	ppm	5.38	5.33	5.58	5.57	11.02	11.4	11.76	11.91	13.33	13.84	12.9	13.14	7.7	7.99	7.8	7.8	2
Co	ppm	21.5	21.8	26	21.5	30.8	27.3	26.5	27	14.9	15.6	14.7	15.3	16.5	18.6	16.3	15.4	2
Ni	ppm	200	211	292	191	372	312	298	300	67	83	61	73	122	125	132	107	7–30
Sr	ppm	174	180	139	140	144	140	150	150	137	144	144	152	140	166	139	144	15
Zr	ppm	50	44	31	38	47	45	50	51	50	47	40	49	47	38	49	46	50
Ba	ppm	59	62	40	37	49	45	51	47	59	64	59	62	89	83	111	135	15
La	ppm	3.5	3.64	2.42	2.37	3.81	3.26	3.61	4.14	3.99	3.96	3.93	3.85	3.25	3.01	3.15	3.51	2
Ce	ppm	8.6	9	6.1	5.9	9.6	8.3	9.1	10.6	10	10	9.8	9.6	8	7.1	7.9	9.2	4
Nd	ppm	5	5.4	4	3.3	5.4	4.7	6.4	7	6.1	5.2	5.3	6.2	4.7	4.7	4.2	5.4	35
Sm	ppm	1.51	1.6	1.09	1.05	1.74	1.55	1.78	2.06	1.8	1.82	1.78	1.78	1.46	1.31	1.34	1.72	2
Eu	ppm	1.03	1.05	0.74	0.72	0.8	0.8	0.8	0.82	0.88	0.87	0.87	0.86	0.81	0.8	0.82	0.83	3
Tb	ppm	0.3	0.33	0.23	0.22	0.37	0.33	0.39	0.44	0.38	0.41	0.39	0.38	0.31	0.29	0.3	0.36	6
Yb	ppm	1.39	1.4	1.01	0.99	1.5	1.41	1.62	1.81	1.7	1.76	1.71	1.68	1.41	1.43	1.39	1.5	2
Lu	ppm	0.193	0.196	0.144	0.139	0.212	0.197	0.224	0.248	0.238	0.248	0.24	0.241	0.198	0.209	0.197	0.209	3
Hf	ppm	1.21	1.26	0.86	0.82	1.5	1.48	1.25	1.45	1.39	1.5	1.44	1.37	1.39	1.23	1.26	1.15	4
Ta	ppm	0.19	0.21	0.16	0.15	0.37	0.25	0.18	0.2	0.21	0.21	0.2	0.2	0.2	0.24	0.12	0.14	15
Ir	ppb	8.8	8.4	8.5	5.6	15.8	14.7	13.7	13.5	3.6	3.7	3.6	4.7	6	6	6.6	6.6	10–40
Au	ppb	1.6	1.8	2.2	<5	5.2	4.8	4.3	4.1	<5	<5	<5	<5	1.1	<5	1.9	2.2	30–90
Th	ppm	0.83	0.88	0.65	0.56	0.91	0.7	0.68	0.88	0.9	0.9	0.92	0.91	1.05	0.64	0.77	1.64	5
U	ppm	0.25	0.26	0.19	0.17	0.27	0.21	0.2	0.25	0.28	0.27	0.29	0.27	0.39	0.21	0.27	0.72	25

5. DISCUSSION

5.1. Ar–Ar ages

The four granulitic breccias studied here have been reprocessed by multiple impacts and, thus, represent second or third generation rocks. In lithologies like the granulitic breccias (and impact-melt breccias), the assembly age of the rock can only be constrained to be the same as, or younger than, that of the youngest clast, while the oldest clast represents the lower limit on the age of the precursor rocks.

The granulitic breccias have experienced at least four major events: (1) crystallization of the parent lithologies represented by mineral and lithic clasts, (2) brecciation and assembly of the parent impact breccia, (3) recrystallization, grain coarsening, and chemical homogenization via thermal metamorphism (at ~1000 °C) to form the granoblastic or poikiloblastic texture and homogeneous mineral compositions diagnostic of this lithology, and (4) excavation, with possible further brecciation and low-temperature overprinting while samples were close to surface.

We will use the step-heating results here since our work has shown that the fine-grained nature of these rocks tends to average the laser spot ages. The geochronological results from sample 78155 are the simplest to interpret, since it yielded an excellent concordant step-heating plateau of 4106 ± 43 Ma. Very minor post-crystallization reheating is indicated by lower ages in the first few steps of the release spectrum. The step-heating release spectrum of sample 79215 yields a flat pattern but with sufficient scatter to fall outside the criteria for a 'plateau' age. A total gas age of 3874 ± 16 Ma and a mean age of 3871 ± 40 Ma (Fig. 5c) indicate the likely age is 3900 ± 100 Ma. This age falls within the generally accepted range of ages for the late heavy bombardment (LHB); thus, it may represent the time at which 79215 was excavated from depth in a large basin-forming impact and juxtaposed with an overlying melt sheet or hot ejecta blanket.

Disturbed spectra indicate that the last events to affect the two remaining samples, 60035 and 77017, were lower temperature overprints, which caused partial argon resetting subsequent to their main metamorphic recrystallization and excavation. These samples both contain a mixture of target-rock clasts and mineral fragments that have a range of argon retention properties and grain sizes. In both cases, the step-heating data is more informative than the laser spot ages, and probably reflects a single anhydrous, fine-grained, potassium-bearing phase that dominates argon release. Similar patterns have been seen in fine-grained plagioclase mineral separates (McDougall and Harrison, 1999).

The oldest ages from 60035 (4088 ± 100 Ma) and 77017 (4106 ± 39 Ma) are similar to those obtained from other granulitic breccias (pre-Nectarian) (Fig. 8), but their release spectra and spot ages reveal later events scattered over billions of years. Sample 60035 suffered 49% argon loss at ~3200 Ma, and 77017 suffered 29% argon loss at ~2300 Ma. The greater susceptibility of samples 60035 and 77017 to partial resetting can be related to their finer grain size (25–100 μm) compared to the coarser grain size of feldspars in samples 78155 and 79215 (up to 200 μm). Samples with smaller grain sizes, high defect densities, or submicroscopic cracks are more likely to lose argon in later events. The presence of shock veins in samples 60035 and 77017, but not in samples 78155 or 79215, also suggests the former were affected by post-peak metamorphic impact events. We equate the younger ages of 60035 and 77017 to resetting by processes (impacts and related hot burial) occurring close to the lunar surface at those times.

5.2. Conditions of post-Imbrian thermal overprinting

In order to constrain the post-peak metamorphic processes that affected the Ar–Ar ages of the granulitic breccias, we have modeled the amount of argon lost from the two finer-grained samples during later low-temperature events (Fig. 7). The proportion of post-granulite argon loss in these two samples (60035 and 77017) can be calculated using the estimated original age (mean age of the highest temperature steps) and the total gas age. The younger ages are not related to the peak (granulite) metamorphism. Rapid cooling following peak metamorphism is dated by the later release in the step-heating spectra of 60035 and 77017, and by the plateau and mean ages of samples 78155 and 79215. The events responsible for subsequent Ar loss are a function of reheating and grain size. Consequently, we have modeled a range of grain sizes (from 1 to 1000 μm) and temperatures (200–500 °C) in order to establish a plausible regime of thermal overprinting.

Three models for simple (square wave) heating events are shown in Fig. 7. The plot of fractional argon loss against a range of sub-grain sizes illustrates the effects of different temperatures. Diffusion is a logarithmic process and major loss of argon occurs at the peak temperature, so the indicated temperatures are a reasonable first approximation.

Based on an average sub-grain size (roughly 25–50 μm) in 60035 and 77017, our results indicate that the heating events that partially reset the argon chronometers of the finer-grained samples are likely to have been low-temperature. The observed partial resetting can be explained by a heating at 300 °C for 1000 years (perhaps due to the superimposition of a rapidly cooling sheet of hot ejecta), or by longer heating at 250 and 200 °C for 10,000 and 100,000 years, respectively (perhaps representing slightly deeper burial and a location at the periphery of an impact crater or in proximity to a melt sheet). For 60035 and 77017 to cool to these lower temperatures yet retain their observed peak signatures, both must have suffered earlier metamorphism and been close to the surface prior to 4.0 Ga.

5.3. Cooling regimes and equilibration temperatures

Pyroxene equilibration temperatures for the four samples are significantly higher (990–1100 °C) than the temperatures of the later events that caused the argon loss (~200–300 °C), indicating that partial argon loss occurred after the samples were re-equilibrated. We interpret the pyroxene equilibration temperatures to coincide with high-temperature granulite metamorphism, which would have completely reset their argon chronometers.

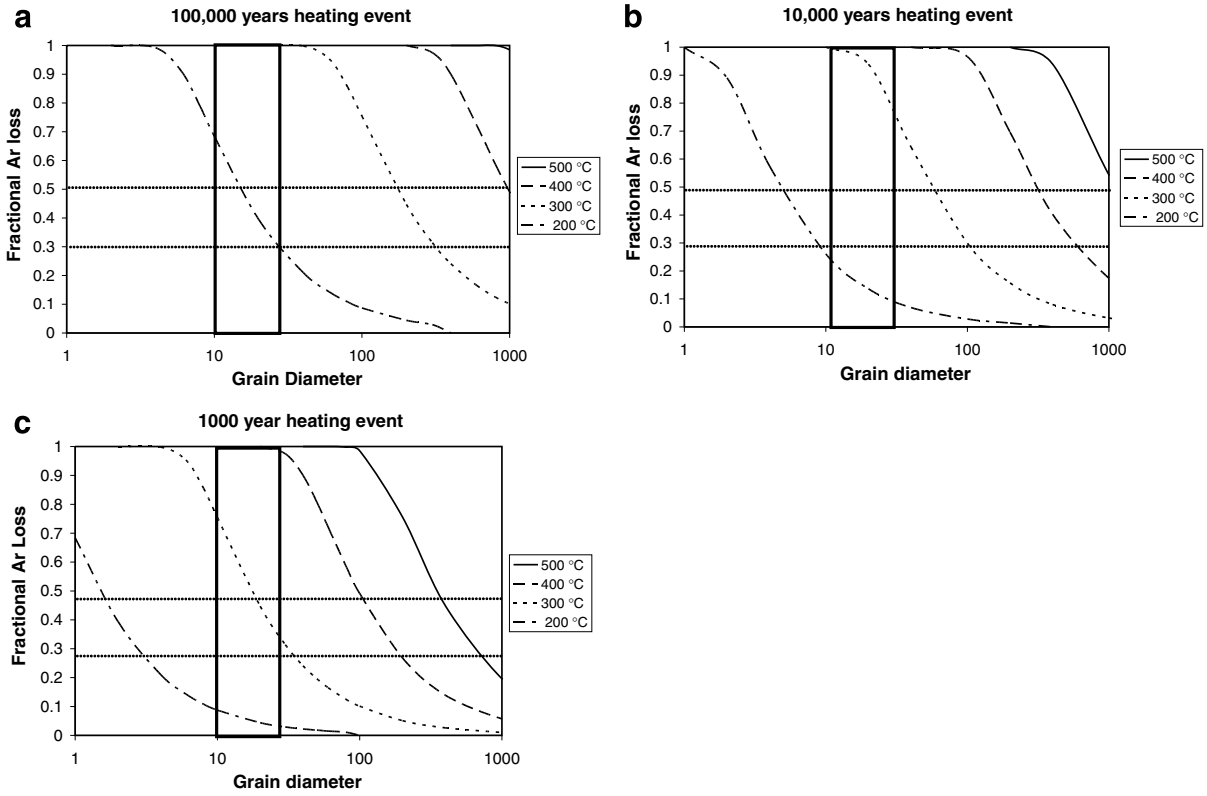

Fig. 7. Cooling regimes for (a) a 100,000 year thermal event, (b) a 10,000 year event, and (c) a 1000 year event based on grain size. The proportional loss from samples 60035 (30% loss) and 77017 (49% loss) is shown as horizontal dotted lines, and the measured range of sub-grain sizes is shown as vertical solid lines. The thick black box constrained by these four lines indicates the possible combination of grain sizes and percent argon lost. Temperature curves within the box indicate the temperature responsible for producing the effects seen in our samples.

If cooling had been rapid and monotonic following the high-temperature granulite event then the Ar–Ar analyses should yield simple step-heating plateau ages. If the rocks had experienced later low-temperature events, then their Ar–Ar spectra should reveal variable resetting and a range of release patterns from complete resetting (a plateau with a younger age), to moderate resetting (the original age may not be preserved), to minor resetting (the original age might only be preserved in some spot ages and in the high-temperature steps of the step-heating spectrum).

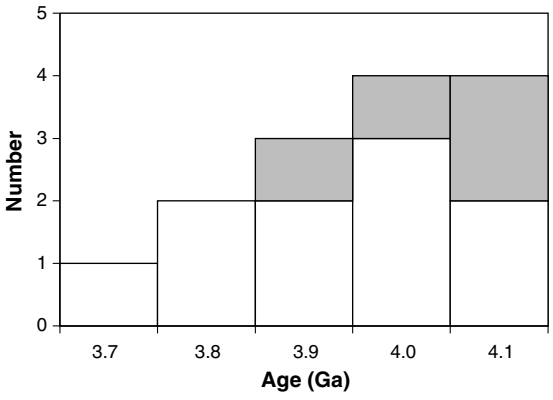

Fig. 8. Relative probability plot of our high-temperature and plateau ages (grey) and ages from the literature (white) for 14 granulitic breccias (see Table 1).

Combining our plateau age and high-temperature ages with the previously published Ar–Ar data (Table 1 and Fig. 8) for the granulitic breccias reveals a range of ages from 3.75 Ga to an abrupt cut-off at 4.1 Ga. This suggests more than one granulite-forming event, assuming that they were short-lived events followed by rapid cooling (Cushing et al., 1999). The population is dominated by ages in the range of 4.1–3.9 Ga, a spread larger than the individual experimental errors in our data and most of the published data. Although some granulite ages in the literature (generally those in abstracts) were quoted without errors, those ages also fall in the middle of the age distribution. Assuming those ages without assigned errors have errors approximating 0.1 Ga, the combined weighted mean age (errors are assigned using the product of student's 't' and square root of the MSWD (Ludwig, 2003)) of the literature data ($n = 10$) is 3.95 ± 0.06 Ga (95% confidence limits), while our data ($n = 4$) yield 4.01 ± 0.15 Ga (95% confidence limits). Further analysis of lunar granulites may resolve a pattern, but the current results indicate that either there were more impacts in the period of 4.1–3.9 Ga, or that many earlier Ar–Ar ages were completely reset at this time. Both interpretations require the continuation of impacts affecting the area near the Imbrium basin (and the Apollo 16 and 17 sites) until

at least 3.75 Ga. The moderately high siderophile content of the granulitic breccias also requires that impact events were occurring before 4.1 Ga (i.e., their parental lithologies needed to be impregnated with siderophiles before high-temperature, granulite-grade metamorphism).

5.4. Cosmic ray exposure ages

The CRE ages of the granulitic breccias (Table 3) cannot be linked to specific crater forming events. However, ejecta from the Tycho impact found at the Apollo 17 site has been dated to be ~100 Ma, based on Apollo 17 samples (Jolliff et al., 1998). With a CRE age of 133 ± 9.5 Ma, sample 77017 may have been affected by the Tycho event. Jolliff et al. (1998) found abundant incompatible trace element-poor granulitic rock fragments within the Tycho ejecta. Several of these samples are ferroan and similar in composition to 77017. The CRE ages of the three other samples do not correspond to any of the young rayed craters at the Apollo 16 and 17 sites (e.g., North Ray, South Ray, Baby Ray).

The dating of lunar glass spherules by Culler et al. (2000) indicates that the lunar cratering rate overall has decreased over the last 3000 Ma. However, the spherule data also suggest a relative increase in cratering events in the last 500 Ma, which is compatible with the CRE ages of the four samples discussed here.

5.5. Geochemistry

The bulk compositions of the granulitic breccias (Table 2) are similar to the average composition of lunar highlands crust (Korotev et al., 2003). Normatively, these rocks are anorthositic norites or anorthositic troctolites (Warner et al., 1977). In contrast to most other Apollo polymict breccias, granulitic breccias have low but variable abundances of incompatible trace elements (Lindstrom and Lindstrom, 1986). The granulitic breccias contain clasts of many different lithologies and appear to be a mixture of FAN and magnesian suite rocks based on major element contents of mineral and lithic fragments (Lindstrom and Lindstrom, 1986) (Fig. 2). However, when trace element compositions are considered, the granulitic breccias lie outside the compositions of all other known lunar rocks (Fig. 9). The trace element compositions of granulitic breccias do not correspond to the magnesian suite norites, troctolites, or trocotolitic anorthosites (or any mixture thereof) found at the Apollo 16 and 17 sites (Korotev and Jolliff, 2001). Granulitic breccias have higher Th/Sm ratios than any other known rock type, despite containing, on average, low absolute concentrations of incompatible elements (Korotev and Jolliff, 2001). Mixing of known igneous and plutonic lunar rocks cannot explain this composition. This suggests that the parental polymict lithologies may have contained clasts of rock types yet to be described from the lunar surface (Korotev and Jolliff, 2001).

There is a linear relationship between meteoritic siderophile element concentration and $^{40}Ar/^{39}Ar$ spot age amongst the dated samples (Fig. 10a and b). As the measured Ar–Ar spot age of the sample decreases, siderophile element concentration increases. There is no relationship between the step-heating age of the sample and siderophile content. As discussed, the two samples

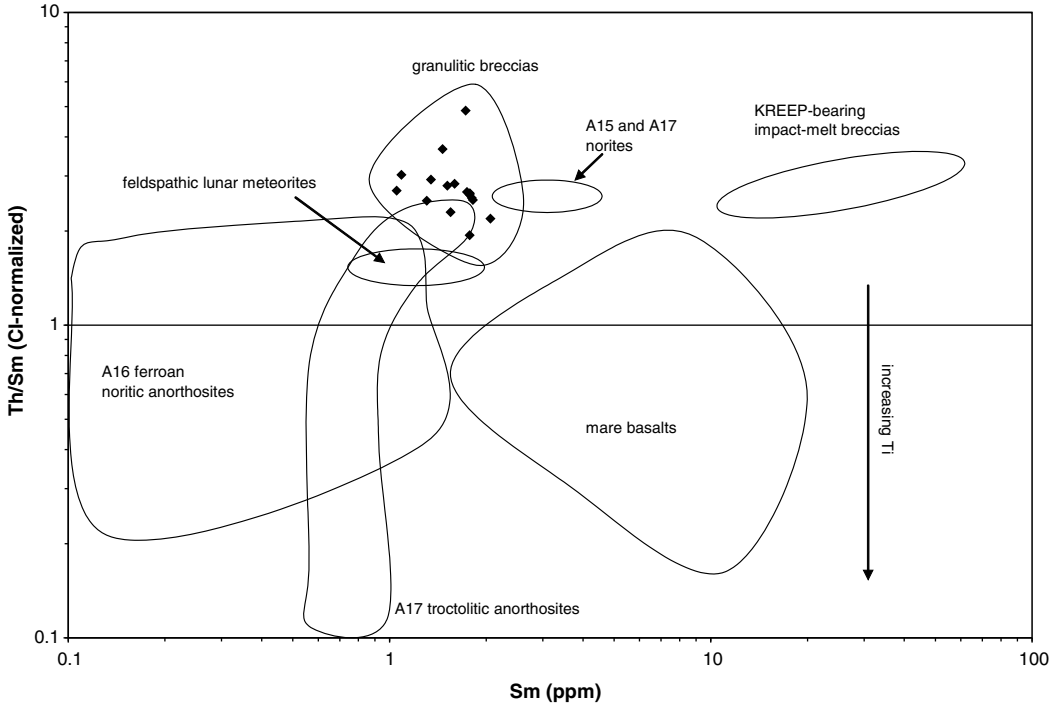

Fig. 9. CI-chondrite-normalized Th/Sm versus Sm concentration for various types of lunar rocks in comparison to our data for the four studied granulitic breccias (black diamonds; data from Table 4). Fields for other rocks types are from Korotev and Jolliff (2001). Granulitic breccias have higher Th/Sm ratios than any other known rock type, despite containing low absolute concentrations of incompatible elements.

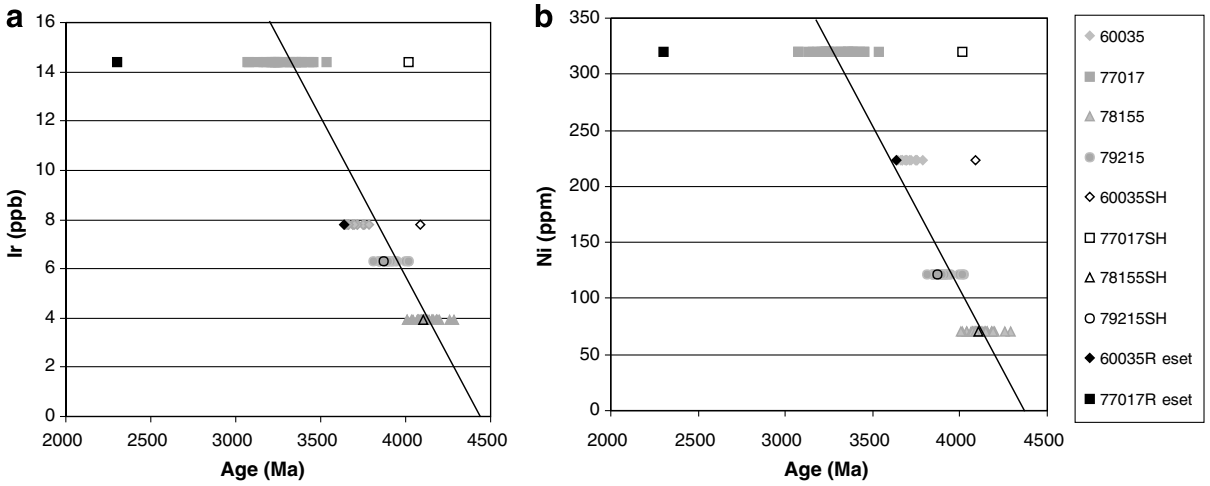

Fig. 10. Siderophile concentrations versus age for the four studied granulitic breccia samples (a) Ir, (b) Ni. Grey-filled symbols represent spot ages, open symbols represent mean step-heating ages or plateau ages, and black symbols represent step-heating ages corresponding to partial resetting of Ar in plagioclase.

yielding younger spot ages (77017 and 60035) probably experienced argon loss as a result of low-temperature overprinting because of their finer grain size. We equate the higher siderophile contents of these samples as being due to their having undergone more impacts prior to peak (granulite) metamorphism and, hence, increased impactor contamination. More impacts would also result in enhanced comminution, which equates with their current finer grain size. However, the fact that 77017 and 60035 retain their dominant high-temperature metamorphic ages indicates that impact-generated comminution and associated siderophile addition must have occurred prior to peak metamorphism. Moreover, the high-temperature thermal event did not totally erase the fine-grained nature of these samples via grain growth (even though it did anneal these rocks). This evidence hints at the finer-grained granulites being derived from pre-4.0 Ga regolith, while the two coarser-grained samples could have been more coherent rocks buried at some depth and so shielded below the effects of near-surface impacts and associated siderophile addition.

6. CONCLUSIONS

Four samples of Apollo granulitic breccias have been mineralogically and geochemically characterized, and high-resolution $^{40}Ar/^{39}Ar$ ratios determined on polished tiles using IR laser single shots and continuous laser step-heating. These results increase the amount of data available for the granulitic breccias and lunar highlands crustal samples in general.

The peak metamorphic conditions (i.e., the granulite-forming event) are associated with ages of 4.1–3.9 Ga. Based on their textures and peak temperatures (1000–1100 °C), we conclude that the source of heat for peak granulite conditions was either superheated impact-melts or associated fallback breccias and ejecta (i.e., via footwall contact metamorphism), rather than deep burial in the lunar crust. In order to maintain temperatures of ~1000 °C to effect solid-state recrystallization and re-equilibration of the rocks, the impact-melts or ejecta blankets responsible for metamorphosing the protoliths of the granulitic breccias must have been relatively substantial and, therefore, were probably associated with larger cratering events (i.e., basin formation).

The four granulitic breccia ages indicate subsequent rapid cooling following peak metamorphism, a plausible mechanism for which is exhumation via impact. In the case of sample 79215, peak metamorphism is dated at 3.9 Ga, which may correlate with formation of the Serenitatis impact basin (Stöffler et al., 2006). The other three samples indicate peak metamorphic ages of ~4.1 Ga. The moderately high concentrations of meteoritic siderophile elements (average 8 ppb Ir) in these three samples provide evidence for pre-4.0 Ga projectile contamination of their protoliths. Partial resetting events that are younger than 3.9 Ga are detected in the two finer-grained granulites. These indicate a greater susceptibility to argon loss during relatively low-temperature reheating due to their grain size and proximity to later melt sheet- or ejecta blanket-forming events.

ACKNOWLEDGMENTS

This work was supported by a Natural Sciences and Engineering Research Council of Canada (NSERC) Canada Graduate Scholarship (D-3) grant and a University of New Brunswick J.S. Little Travel Fellowship awarded to J.A.H.; NSERC and CRC grants to J.G.S., and NASA support to R.L.K. S.P.K. and S.C.S. gratefully acknowledge funding from the Leverhulme Trust (F/00 269/J). The authors thank Vera Fernandes, two anonymous reviewers and Associate Editor David Mittlefehldt for commenting on an earlier version of the manuscript. We also thank Vera Fernandes for the use of her algorithm for calculating cosmic ray exposure ages. Samples were allocated to J.G.S. by NASA's Johnson Space Center. PASSC contribution 56.

APPENDIX A

Laser spot analyses

Sample	Spot	$^{38}Ar/^{39}Ar$	$^{37}Ar/^{39}Ar$	$^{36}Ar/^{39}Ar$	^{39}Ar	$^{40*}Ar/^{39}Ar$	±	Laser spot age (Ma)	±(1σ)
60035	1	0.07	133.28	0.05	0.01	206.36	1.46	3755	27
60035	2	0.07	144.86	0.05	0.01	193.88	0.56	3657	18
60035	3	0.07	119.20	0.06	0.01	205.40	0.82	3748	20
60035	4	0.08	169.25	0.07	0.00	198.11	2.14	3691	37
60035	5	0.05	64.44	0.05	0.02	201.61	0.79	3718	20
60035	6	0.07	118.39	0.06	0.00	197.73	1.95	3688	35
60035	7	0.08	145.41	0.05	0.00	205.61	2.13	3749	36
60035	8	0.07	73.22	0.05	0.01	191.57	2.12	3638	38
60035	9	0.07	117.47	0.05	0.01	201.24	0.72	3716	19
60035	10	0.04	92.06	0.04	0.01	210.02	2.17	3783	36
60035	11	0.08	157.71	0.04	0.00	198.82	1.81	3697	33
60035	12	0.06	105.27	0.05	0.01	195.03	1.44	3666	28
60035	13	0.08	95.13	0.06	0.01	194.97	0.82	3666	20
60035	14	0.08	168.57	0.06	0.00	192.35	1.00	3645	23
77017	1	1.25	114.23	1.04	0.00	154.70	3.19	3309	64
77017	2	1.13	106.68	0.82	0.00	148.66	1.28	3249	30
77017	3	1.25	118.41	1.00	0.00	150.96	0.59	3272	19
77017	4	1.53	128.39	1.09	0.00	147.97	1.02	3242	26
77017	5	1.49	123.00	0.99	0.00	145.54	0.68	3217	21
77017	6	1.09	97.08	0.79	0.01	169.82	0.82	3451	21
77017	7	1.20	82.82	0.87	0.01	140.07	0.37	3160	17
77017	8	1.37	131.76	1.06	0.00	170.20	0.87	3455	22
77017	9	1.28	110.39	0.95	0.01	147.20	1.39	3234	32
77017	10	1.33	116.26	1.06	0.01	137.49	0.33	3132	16
77017	11	1.35	91.34	1.01	0.00	161.07	0.87	3370	22
77017	12	1.30	107.33	0.98	0.00	142.15	0.68	3182	21
77017	13	1.44	123.42	1.11	0.00	178.90	1.34	3532	28
77017	14	1.04	79.65	0.77	0.01	144.89	0.36	3210	17
77017	15	1.28	108.05	0.94	0.00	163.06	1.02	3389	24
77017	16	1.47	111.60	1.01	0.00	157.69	1.46	3338	32
77017	17	1.26	104.98	0.92	0.01	162.54	0.99	3384	24
77017	18	1.45	124.95	1.08	0.01	167.13	0.55	3427	18
77017	19	1.39	138.62	1.01	0.01	132.06	0.43	3072	18
77017	20	1.25	104.86	0.84	0.01	159.69	1.35	3357	30
77017	21	1.05	84.86	0.82	0.01	146.06	0.51	3222	18
77017	22	1.01	91.17	0.75	0.01	159.48	1.40	3355	31
77017	23	1.58	132.70	1.13	0.01	155.70	0.52	3319	18
77017	24	1.30	104.72	0.94	0.01	132.22	0.40	3074	17
77017	25	1.21	78.86	0.92	0.01	147.39	0.92	3236	24
77017	26	0.90	78.78	0.77	0.01	149.01	0.58	3252	19
77017	27	1.44	115.64	0.99	0.01	163.27	0.94	3391	23
78155	1	0.14	72.25	0.10	0.01	261.12	0.53	4132	18
78155	2	0.13	68.51	0.11	0.01	259.59	0.70	4122	18
78155	3	0.13	65.11	0.11	0.01	264.92	0.79	4155	19
78155	4	0.14	74.12	0.11	0.02	264.28	0.58	4151	18
78155	5	0.16	75.89	0.11	0.00	256.57	1.81	4103	28
78155	6	0.16	84.64	0.12	0.00	262.18	1.80	4139	28
78155	7	0.13	74.14	0.10	0.01	252.95	0.46	4080	17
78155	8	0.15	72.35	0.11	0.02	253.65	0.73	4085	19
78155	9	0.14	63.49	0.10	0.01	255.50	1.05	4097	21
78155	10	0.13	68.11	0.11	0.01	265.62	0.49	4160	17
78155	11	0.15	75.50	0.12	0.01	272.37	1.66	4201	26
78155	12	0.14	75.25	0.11	0.02	269.06	0.69	4181	18
78155	13	0.14	65.86	0.12	0.01	255.42	0.70	4096	18
79215	1	1.37	49.96	1.02	0.00	218.87	1.28	3848	25
79215	2	1.55	49.32	1.04	0.00	232.85	2.92	3947	43
79215	3	1.76	59.50	1.03	0.00	243.71	3.57	4020	50
79215	4	1.53	51.38	1.07	0.01	229.15	1.64	3922	28

(*continued on next page*)

Appendix A (*continued*)

Sample	Spot	$^{38}Ar/^{39}Ar$	$^{37}Ar/^{39}Ar$	$^{36}Ar/^{39}Ar$	^{39}Ar	$^{40*}Ar/^{39}Ar$	±	Laser spot age (Ma)	±(1σ)
79215	5	1.45	44.39	1.03	0.01	231.20	0.94	3936	21
79215	6	1.44	48.44	1.01	0.01	224.20	0.97	3887	21
79215	7	1.36	43.52	0.97	0.01	229.56	1.20	3924	23
79215	8	1.42	32.83	1.04	0.01	224.12	2.05	3886	33
79215	9	1.48	54.71	1.01	0.01	223.55	1.62	3882	28
79215	10	1.46	47.37	1.05	0.01	226.56	1.92	3903	31
79215	11	1.52	54.96	1.01	0.01	223.37	1.20	3881	23
79215	12	1.54	50.20	1.06	0.01	240.27	1.56	3998	26
79215	13	1.33	49.99	0.93	0.01	225.93	1.06	3899	22
79215	14	1.39	46.16	0.98	0.01	218.35	0.78	3845	20
79215	15	1.48	50.93	1.13	0.01	242.89	1.04	4015	21
79215	16	1.43	50.31	0.95	0.01	218.88	0.90	3849	21
79215	17	1.57	52.54	1.01	0.01	214.02	0.82	3813	20
79215	18	1.45	45.58	1.05	0.01	227.67	0.95	3911	21
79215	19	1.41	46.81	0.99	0.01	225.97	0.59	3899	18
79215	20	1.38	50.27	1.01	0.01	221.87	1.36	3870	25
Step-heating experiments									
60035	1	0.04	−230.37	0.18	0.00	147.51	19.67	3237	201
60035	2	0.06	−1356.85	0.68	0.00	20.06	25.46	938	929
60035	3	0.07	−51.40	0.07	0.00	177.36	29.85	3518	261
60035	4	0.04	19.43	0.05	0.00	186.30	3.27	3595	28
60035	5	0.06	−4.02	0.06	0.00	203.07	8.08	3730	63
60035	6	0.04	34.65	0.02	0.00	205.54	6.41	3749	50
60035	7	0.07	110.68	0.06	0.00	236.97	17.29	3975	117
60035	8	0.04	137.39	0.02	0.00	225.02	14.56	3893	104
60035	9	0.02	113.64	0.04	0.00	245.82	30.68	4034	201
60035	10	0.08	203.48	0.04	0.00	222.09	15.42	3872	111
60035	11	0.08	154.62	0.06	0.00	223.71	7.66	3883	55
60035	12	0.06	293.61	0.08	0.00	252.23	16.27	4076	105
60035	13	0.06	218.17	0.03	0.00	250.92	9.18	4067	60
60035	14	0.19	507.88	0.17	0.00	302.93	37.07	4375	201
77017	1	3.14	3652.04	1.27	0.00	164.15	33.29	3399	310
77017	2	12.21	16884.60	4.03	0.00	572.52	698.20	5446	2093
77017	3	1.27	363.15	0.80	0.00	78.26	2.52	2341	43
77017	4	1.09	80.69	0.76	0.01	99.55	2.12	2667	30
77017	5	1.09	107.20	0.76	0.01	146.46	3.44	3226	36
77017	6	1.23	176.38	0.77	0.00	184.24	9.15	3577	78
77017	7	1.15	78.79	0.75	0.00	201.46	7.54	3717	59
77017	8	1.13	−18.15	0.84	0.00	212.35	10.11	3800	76
77017	9	1.24	29.18	0.94	0.00	233.06	10.70	3949	74
77017	10	1.35	158.10	0.99	0.00	254.65	21.43	4091	136
77017	11	1.29	80.38	0.95	0.00	244.58	10.47	4026	69
77017	12	1.48	109.73	1.04	0.00	246.46	11.61	4039	76
77017	13	1.35	117.71	0.97	0.00	257.25	18.32	4108	116
77017	14	1.30	74.44	0.88	0.00	237.64	19.63	3980	133
77017	15	1.15	25.55	0.82	0.01	238.51	3.91	3986	28
77017	16	1.52	70.06	1.10	0.00	254.53	7.52	4091	48
77017	17	1.25	40.28	0.88	0.00	236.12	8.90	3970	61
77017	18	1.46	351.59	0.96	0.00	289.83	42.36	4302	239
78155	1	0.12	60.46	0.24	0.00	246.01	4.40	4036	60
78155	2	0.09	58.32	0.11	0.00	287.27	3.48	4287	43
78155	3	0.06	51.33	0.12	0.00	247.05	2.89	4042	41
78155	4	0.13	54.40	0.09	0.01	242.04	1.69	4009	28
78155	5	0.12	69.62	0.08	0.02	258.52	0.90	4116	20
78155	6	0.15	70.34	0.10	0.01	257.08	0.49	4107	17
78155	7	0.14	76.70	0.10	0.01	258.55	0.94	4116	20
78155	8	0.13	66.62	0.10	0.01	256.65	0.86	4104	20
78155	9	0.14	72.50	0.10	0.01	251.98	1.95	4074	30
78155	10	0.17	62.72	0.11	0.01	256.12	1.04	4101	21
78155	11	0.12	58.86	0.11	0.00	269.23	4.51	4182	57
78155	12	0.19	79.92	0.12	0.00	257.51	2.02	4109	30

Appendix A (*continued*)

Sample	Spot	$^{38}Ar/^{39}Ar$	$^{37}Ar/^{39}Ar$	$^{36}Ar/^{39}Ar$	^{39}Ar	$^{40*}Ar/^{39}Ar$	±	Laser spot age (Ma)	±(1σ)
78155	13	0.16	79.07	0.12	0.01	253.03	0.96	4081	20
78155	14	0.16	78.59	0.11	0.00	264.22	1.12	4151	21
78155	15	0.16	94.98	0.15	0.00	250.79	2.59	4067	37
78155	16	0.17	93.39	0.15	0.00	251.57	2.32	4072	34
78155	17	0.15	88.36	0.17	0.00	254.53	6.34	4091	82
78155	18	0.16	77.85	0.14	0.00	241.63	2.07	4007	32
78155	19	0.17	107.75	0.20	0.00	281.92	5.57	4257	67
78155	20	0.17	87.81	0.19	0.00	270.85	2.48	4191	34
79215	1	1.34	12.50	0.88	0.01	217.33	1.59	3837	14
79215	2	1.23	−165.62	0.86	0.00	196.20	8.92	3676	72
79215	3	1.43	−30.42	0.89	0.00	229.85	4.08	3927	29
79215	4	1.40	42.50	0.88	0.02	219.94	0.86	3856	10
79215	5	1.49	39.28	0.99	0.03	226.00	1.09	3900	11
79215	6	1.45	58.75	0.95	0.01	225.23	1.60	3894	14
79215	7	1.47	10.91	0.96	0.01	223.50	2.24	3882	18
79215	8	1.58	26.44	1.05	0.02	225.33	1.50	3895	13
79215	9	1.95	55.37	1.35	0.02	220.01	0.96	3857	11
79215	10	1.93	25.10	1.29	0.01	216.25	1.44	3829	13
79215	11	1.76	96.00	1.17	0.01	223.08	3.29	3879	25
79215	12	1.97	77.59	1.30	0.01	231.73	3.33	3940	24

REFERENCES

Bickel C. E. (1977) Petrology of 78155: an early, thermally metamorphosed polymict breccia. *Proc. Lunar Sci. Conf.* **8**, 2007–2027.

Bickel C. E. and Warner J. L. (1978) Survey of plutonic and granulitic lithic fragments. *Proc. Lunar Sci. Conf.* **9**, 629–652.

Bickel C. E., Warner J. L. and Phinney W. C. (1976) Petrology of 79215: brecciation of a lunar cumulate. *Proc. Lunar Sci. Conf.* **7**, 1793–1819.

Brey G. P. and Köhler T. (1990) Geothermobarometry in four-phase lherzolites II. New thermobarometers, and practical assessment of existing thermobarometers. *J. Petrol.* **31**, 1353–1378.

Cadogan P. H. and Turner G. (1976) The chronology of the Apollo 17 station 6 boulder. *Proc. Lunar Sci. Conf.* **7**, 2267–2285.

Cohen B. A. (2004) Can granulite metamorphic conditions reset ^{40}Ar–^{39}Ar ages in lunar rocks? *Lunar Planet. Sci. XXXV*. Lunar Planet. Inst., Houston. CD-ROM #1009 (abstr).

Culler T. S., Becker T. A., Muller R. A. and Renne P. R. (2000) Lunar impact history from ^{40}Ar–^{39}Ar dating of glass spherules. *Science* **287**, 1785–1788.

Cushing J. A., Taylor G. J., Norman M. D. and Keil K. (1999) The granulitic impactite suite: impact melts and metamorphic breccias of the early lunar crust. *Meteor. Planet. Sci.* **34**, 185–195.

Eberhardt P., Geiss J., Graf H., Grögler N., Krähenbühl U., Schwaller H., Schwarzmüller J. and Stettler A. (1970) Trapped solar wind noble gases, $^{81}Kr/Kr$ exposure ages and K/Ar ages in Apollo 11 lunar material. *Science* **167**, 558–560.

Elkins-Tanton L. T., Hager B. H. and Grove T. L. (2004) Magmatic effects of the lunar late heavy bombardment. *Earth Planet. Sci. Lett.* **222**, 17–27.

Eugster O. (2003) Cosmic-ray exposure ages of meteorites and lunar rocks and their significance. *Chem. Erde* **63**, 3–30.

Hertogen J., Janssens M.-J., Takahashi H., Palme H. and Anders E. (1977) Lunar basins and craters: evidence for systematic compositional changes of the bombarding population. *Proc. Lunar Sci. Conf.* **8**, 17–45.

James O. B. (1980) Rocks of the early lunar crust. *Proc. Lunar Sci. Conf.* **11**, 365–393.

James O. B. and Hammarstrom J. G. (1977) Petrology of four clasts from consortium breccia 73215. *Proc. Lunar Sci. Conf.* **8**, 2459–2494.

Jolliff B. L., Korotev R. L. and Haskin L. A. (1998) The Apollo 17 central crater cluster and a new look at possible Tycho components in the soil. *Lunar Planet. Sci. XXIX*. Lunar Planet. Inst., Houston, #1734 (abstr.).

Korotev R. L. (1991) Geochemical stratigraphy of two regolith cores from the Central Highlands of the Moon. *Proc. Lunar Sci. Conf.* **21**, 229–289.

Korotev R. L. and Jolliff B. L. (2001) The curious case of the lunar magnesian granulitic breccias. *Lunar Planet. Sci. XXXII*. Lunar Planet. Inst., Houston. CD-ROM #1455 (abstr.).

Korotev R. L., Jolliff B. L., Zeigler R. A., Gillis J. J. and Haskin L. A. (2003) Feldspathic lunar meteorites and their implications for compositional remote sensing of the lunar surface and the composition of the lunar crust. *Geochim. Cosmochim. Acta* **67**, 4895–4923.

Kirsten T. and Horn P. (1974) Chronology of the Taurus-Littrow region III—ages of mare basalts and highland breccias and some remarks about the interpretation of lunar highland rock ages. *Proc. Lunar Sci. Conf.* **5**, 1451–1475.

Lindstrom M. and Lindstrom D. (1986) Lunar granulites and their precursor anorthositic norites of the early lunar crust. *J. Geophys. Res.* **91**, 263–276.

LSPET (1973) The Apollo 16 lunar samples: petrographic and chemical description. *Science* **17**, 23–33.

Ludwig K. R. (2003) Isoplot 3.00. *Berkeley Geochronology Center, Spec. Publ.* No. **4**, 70 pp.

Ma M.-S. and Schmitt R. A. (1982) Chemistry of the matrix, glass coating and an olivine clast from polymict ANT breccia 60035. *Lunar Planet. Sci. XIII*. Lunar Planet. Inst., Houston. 453–454.

Marvin U. B., Lindstrom M. M., Bernatowicz T. J., Podosek F. A. and Sugiura N. (1987) The composition and history of breccia 67015 from North Ray Crater. *Proc. Lunar Sci. Conf.* **17**, in *J. Geophys. Res.* **92**, E471–E490. Lunar and Planetary Institute Publication.

McDougall I. and Harrison T. M. (1999) *Geochronology and Thermochronology by the $^{40}Ar/^{39}Ar$ Method*. Oxford University Press, 269pp.

McGee J. J., Bence A. E. and Schaeffer O. A. (1978) Feldspathic granulite 79215: conditions of metamorphism and age. *Proc. Lunar Sci. Conf.* **9**, 720–722.

Meyer C. (1994) *Catalog of Apollo 17 Rocks, Volume 4*. Johnson Space Center Curatorial Branch Publication 87.

Nunes P. D., Tatsumoto M. and Unruh D. M. (1975) U–Th–Pb systematics of anorthositic gabbros 78155 and 77017—implications for early lunar evolution. *Proc. Lunar Sci. Conf.* **6**, 1445–1465.

Oberli F., Huneke J. C., McCulloch M. T., Papanastassiou D. A. and Wasserburg G. J. (1979) Isotopic constraints for the early evolution of the Moon. *Meteoritics* **14**, 502–503.

Papike J. J., Ryder G. and Shearer C. K. (1998) Lunar samples. In *Planetary Materials. Reviews in Mineralogy and Geochemistry*, vol. 36 (ed. J. J. Papike), pp. 5–234. Planetary Materials. Reviews in Mineralogy and Geochemistry. Mineralogical Society of America, Washington, DC.

Phinney D., Kahl S. B. and Reynolds J. H. (1975) ^{40}Ar–^{39}Ar dating of Apollo 16 and 17 rocks. *Proc. Lunar Sci. Conf.* **6**, 1593–1608.

Steiger R. J. and Jäger E. (1977) Subcommission on geochronology: convention on the use of decay constants in geo- and cosmochronology. *Earth Planet. Sci. Lett.* **36**, 359–362.

Stettler A., Eberhardt P., Geiss J., Grögler N. and Maurer P. (1973) ^{40}Ar–^{39}Ar ages and^{37}Ar–^{38}Ar exposure ages of lunar rocks. *Proc. Lunar Sci. Conf.* **4**, 1865–1888.

Stöffler D., Ryder G., Ivanov B. A., Cintala M. J. and Grieve R. A. F. (2006) Cratering history and lunar chronology. In *New Views of the Moon. Reviews in Mineralogy and Geochemistry*, vol. 60 (eds. B. L. Jolliff, M. A. Wieczorek, C. K. Shearer and C. R. Neal), pp. 519–588. New Views of the Moon. Reviews in Mineralogy and Geochemistry. Mineralogical Society of America, Chantilly, Virginia.

Turner G. (1970) Argon-40/argon-39 dating of lunar rock samples. *Science* **167**, 466.

Turner G. and Cadogan P. H. (1975) The history of lunar bombardment inferred from Ar-40–Ar-39 dating of highland rocks. *Proc. Lunar Sci. Conf.* **6**, 1509–1538.

Warner J. L., Bickel C. E., Phinney W. C. and Simonds C. H. (1977) Feldspathic, granulitic impactites that pre-date the final lunar bombardment. *Proc. Lunar Sci. Conf.* **8**, 979–981.

Warren P. H., Taylor G. J., Keil K., Kalleyman G. W., Rosener P. S. and Wasson J. T. (1983) Sixth foray for pristine non-mare rocks and an assessment of the diversity of lunar anorthosites. *Proc. Lunar Planet. Sci. Conf.* **14**, in *J. Geophys. Res.* **88**, A615–A630.

Wasson J. T. and Kallemeyn G. W. (1988) Compositions of chondrites. *Philos. Trans. R. Soc. Lond.* **325**, 535–544.

Weilerm R. (2002) Cosmic-ray-produced noble gases in meteorites. In *Noble Gases. Reviews in Mineralogy and Geochemistry*, vol. 47 (eds. D. P. Porcelli, C. J. Ballentine and R. Weiler), pp. 125–170. Noble Gases. Reviews in Mineralogy and Geochemistry. Mineralogical Society of America, Washington, DC.

Associate editor: David W. Mittlefehldt